

# SDSS J001153.08-064739.2, a cataclysmic variable with an evolved donor in the period gap<sup>★</sup>

A. Rebassa-Mansergas<sup>1</sup>, S.G. Parsons<sup>2</sup>, C.M. Copperwheat<sup>3</sup>, S. Justham<sup>4</sup>, B.T. Gänsicke<sup>5</sup>,  
M.R. Schreiber<sup>2,6</sup>, T.R. Marsh<sup>5</sup>, V.S. Dhillon<sup>7</sup>

Received \_\_\_\_\_; accepted \_\_\_\_\_

To appear in ApJ

---

★ Based in part on observations made with NTT/Ultracam under program 087.D-0557, and Magellan Clay/MIKE.

<sup>1</sup>Kavli Institute for Astronomy and Astrophysics, Peking University, Beijing 100871, PR China.

<sup>2</sup>Departamento de Física y Astronomía, Universidad de Valparaíso, Valparaíso, Chile.

<sup>3</sup>Astrophysics Research Institute, Liverpool John Moores University, IC2, Liverpool Science Park, 146 Brownlow Hill, Liverpool L3 5RF, UK.

<sup>4</sup>National Astronomical Observatories, Chinese Academy of Sciences, 100012 Beijing, PR China.

<sup>5</sup>Department of Physics, University of Warwick, Coventry CV4 7AL, UK.

<sup>6</sup>Millennium Nucleus "Proto-planetary Disks in ALMA Early Science", Universidad de Valparaíso, Avenida Gran Bretaña 1111, Valparaíso, Chile.

<sup>7</sup>Department of Physics and Astronomy, University of Sheffield, Sheffield, S3 7RH.

## ABSTRACT

Secondary stars in cataclysmic variables (CVs) follow a well defined period-density relation. Thus, canonical donor stars in CVs are generally low-mass stars of spectral type M. However, several CVs have been observed containing secondary stars which are too hot for their inferred masses. This particular configuration can be explained if the donor stars in these systems underwent significant nuclear evolution before they reached contact. In this paper we present SDSS J001153.08-064739.2 as an additional example belonging to this peculiar type of CV and discuss in detail its evolutionary history. We perform spectroscopic and photometric observations and make use of available Catalina Real-Time Transient Survey photometry to measure the orbital period of SDSS J001153.08-064739.2 as 2.4 hours and estimate the white dwarf ( $M_{\text{wd}} > 0.65M_{\odot}$ ) and donor star ( $0.21M_{\odot} < M_{\text{don}} < 0.45M_{\odot}$ ) masses, the mass ratio ( $q = 0.32 \pm 0.08$ ), the orbital inclination ( $47^{\circ} < i < 70^{\circ}$ ), derive an accurate orbital ephemeris ( $T_0 = 2453383.578(1) + E \times 0.10028081(8)$ ), and report the detection of an outburst. We show that SDSS J001153.08-064739.2 is one of the most extreme cases in which the donor star is clearly too hot for its mass. SDSS J001153.08-064739.2 is therefore not only a peculiar CV containing an evolved donor star but also an accreting CV within the period gap. Intriguingly, approximately half of the total currently-observed sample of these peculiar CVs are located in the period gap with nearly the same orbital period.

*Subject headings:* (stars:) novae, cataclysmic variables; (stars:) white dwarfs; stars: low-mass; (stars:) binaries (including multiple): close

## 1. Introduction

A cataclysmic variable (CV) is a close compact binary star formed by a white dwarf primary and a low-mass near-main-sequence secondary star (see Knigge et al. 2011 for a recent review). In non-magnetic CVs the companion transfers material to the white dwarf primary via Roche-lobe overflow and an accretion disk is formed around the white dwarf.

The orbital periods ( $P_{\text{orb}}$ ) of CVs decrease as a consequence of orbital angular momentum loss (AML). The two mechanisms that are thought to drive AML are magnetic wind braking of the donor star (Verbunt & Zwaan 1981) and gravitational radiation (Paczynski 1981), the former several orders of magnitude stronger than the latter. Once the secondary becomes fully convective ( $P_{\text{orb}} \sim 3$  hours) magnetic braking is greatly reduced (Rappaport et al. 1983; Schreiber et al. 2010; Rebassa-Mansergas et al. 2013b) causing the secondary to detach from its Roche-lobe in the 2–3 hour orbital period range known as the period gap (see the orbital period distribution by e.g. Gänsicke et al. 2009). At this stage the evolution becomes much slower, as the AML is mainly driven by gravitational radiation. At  $P_{\text{orb}} \sim 2$  hours the shrinking Roche-lobe comes back into contact with the secondary star and mass transfer is resumed at a much lower rate. Once the secondary star becomes degenerate ( $P_{\text{orb}} \sim 80$  minutes), the overall mass-radius relation for the donor star changes such that it becomes larger upon mass loss. Therefore, the orbital period increases with further mass transfer and the binary orbit widens (Rappaport et al. 1982; Littlefair et al. 2006b).

The secondary stars of CVs with orbital periods below  $\sim 6$  hours are apparently un-evolved M-dwarf main sequence stars, as expected from the well known orbital period-density relation for Roche-lobe filling stars (Knigge et al. 2011). However, several CVs have been recently identified harbouring secondary stars that are too hot for their masses: V 485 ( $P_{\text{orb}} = 59$  minutes, Augusteijn et al. 1996), EIPSc (also known as

RXJ 2329+0628,  $P_{\text{orb}} = 64$  minutes, Thorstensen et al. 2002b), QZ Serpentis ( $P_{\text{orb}} = 2$  hours, Thorstensen et al. 2002a), SDSS J013701.06-091234.9 ( $P_{\text{orb}} = 84$  minutes, Imada et al. 2006), SDSS J170213.26+322954.1 ( $P_{\text{orb}} = 2.4$  hours, Littlefair et al. 2006a), CSS J134052.0+151341 ( $P_{\text{orb}} = 2.45$  hours, Thorstensen 2013), GALEX J194419.33+491257.0 ( $P_{\text{orb}} = 76$  minutes, Kato & Osaki 2014). A few examples exist of longer orbital period CVs that contain secondary stars that are also too hot for their masses (AE Aquarii,  $P_{\text{orb}} = 9.9$  hours, Schenker et al. 2002; HS 0218+3229,  $P_{\text{orb}} = 7.1$  hours, Rodríguez-Gil et al. 2009). It has been suggested that the current peculiar configuration of these systems can be explained if the secondary stars underwent considerable nuclear evolution – i.e. they were nearing the end of the main sequence – before they began to transfer mass onto the white dwarfs (Beuermann et al. 1998; Baraffe & Kolb 2000; Podsiadlowski et al. 2003). In this scenario these more evolved donor stars were initially more massive than typical CV donors and likely underwent a phase of intense thermal-timescale mass transfer. Under these circumstances, the accreted material from the evolved donors should reflect in a different composition compared to canonical CVs, i.e. due to CNO-processes we expect depletion of carbon versus nitrogen. Indeed, unusually high N v / C iv line flux ratios have been observationally confirmed in ultraviolet spectra of (Gänsicke et al. 2003) and QZ Serpentis (Gänsicke 2004). However, it has to be stressed that such a phase of mass transfer is not the underlying cause of the later unusual appearance of the donor stars, as many canonical CVs have also potentially passed through a phase of thermal timescale mass transfer (Schenker et al. 2002).

In the course of our search for white dwarf-main sequence binaries (Rebassa-Mansergas et al. 2010, 2012, 2013a) in the Sloan Digital Sky Survey (SDSS; Abazajian et al. 2009; Aihara et al. 2011) we discovered SDSS J001153.08-064739.2 (hereafter SDSS J0011-0647) and we here present this object as a new system belonging to this peculiar type of CV. We show that SDSS J0011-0647 is one of the most extreme cases in which the secondary star

is far too hot for its mass. The SDSS spectrum of SDSS J0011-0647 is shown in Figure 1. The overall shape of the spectrum is blackbody-like, however reveals broad, double peaked Balmer emission lines, characteristic of an accretion disk, and a very strong Mg I absorption feature near  $5150\text{\AA}$ . This latter feature is the main absorption complex in mid-K stars, which we attribute to the donor star of SDSS J0011-0647. No obvious white dwarf features however can be identified. The SDSS *ugriz* magnitudes of SDSS J0011-0647 are 19.0, 17.8, 17.1, 16.9, and 16.8 respectively.

## 2. Observations

In this section we briefly describe the telescope/instrumentation used for the follow-up observations of SDSS J0011-0647, and outline the reduction of the data.

### 2.1. Spectroscopy

Time-resolved high-resolution spectroscopy of SDSS J0011-0647 was obtained along the 25th of June 2011 and the 22nd and 23rd of September 2012 with the Magellan Inamori Kyocera Echelle (MIKE) spectrograph on the 6.5m Clay Telescope at Las Campanas Observatory. The CCD of MIKE’s red arm has a pixel scale of  $0.13''/\text{pixel}$ , therefore we binned the detector by a factor of three in the dispersion direction and a factor of two in the spatial direction, thus reducing the readout time and readout noise. This, together with a  $1''$  slit, provided access to the  $5200\text{-}9000\text{\AA}$  wavelength range at a resolving power of 22,000 (i.e.  $0.3\text{\AA}$  at the location of the  $\text{H}\alpha$  line). A total of 20 spectra were obtained for SDSS J0011-0647, with exposure times of 600 seconds. The data analysis (reduction and wavelength calibration) was carried out with the *IRAF* software using the standard *IRAF* package *IMRED : ECHELLE*.

## 2.2. Photometry

SDSS J0011-0647 was observed with the high-speed camera ULTRACAM (Dhillon et al. 2007) mounted as a visitor instrument on the ESO 3.5m New Technology Telescope (NTT) at La Silla, Chile on the 24th and 25th of May 2011. ULTRACAM consists of three frame transfer CCDs allowing one to obtain simultaneous photometry in three different filters. For our observations of SDSS J0011-0647 we used the  $u'$ ,  $g'$  and  $r'$  filters. On both nights the seeing was poor ( $>2''$ ) and the moon virtually full, hence we used relatively long exposure times of 10 seconds (the dead-time between the 10 second ULTRACAM exposures was only 25 ms). We obtained just over an hour of photometry on the first night and almost two hours on the second night.

All the data were bias subtracted, flat-fielded and extracted using the ULTRACAM pipeline (Dhillon et al. 2007). The source flux was determined with aperture photometry using a variable aperture, whereby its radius was scaled according to the full width at half maximum. Variations in observing conditions were accounted for by determining the flux relative to several comparison stars in the field of view.

Additional photometry of SDSS J0011-0647 was available from the Catalina Real-Time Transient Survey (CRTS, Drake et al. 2009). We performed differential photometry on the reduced (bias-subtracted and flat-fielded) CRTS images following the routine described by Parsons et al. (2013). Our obtained  $r$ -band light curve is shown in Figure 2. The CRTS photometry spans a time interval of  $\sim 9$  years and reveals an increase of  $\sim 2$  magnitudes at HJD  $\sim 2454400$  days. We interpret this effect as SDSS J0011-0647 undergoing an outburst, which clearly confirms the CV nature of SDSS J0011-0647.

### 3. Results

Here we make use of the spectroscopic and photometric data outlined in the previous section to obtain the orbital and stellar parameters of SDSS J0011-0647.

#### 3.1. Orbital period and semi-amplitude velocity of the donor star

We made use of the long time coverage of the CRTS photometric data ( $\sim 9$  years, see Section 2.2) to determine a precise value of the orbital period of SDSS J0011-0647. We did this as followed. We first run an ORT periodogram (Schwarzenberg-Czerny 1996) to the CRTS data and folded the CRTS magnitudes over the best value of the orbital period obtained from the periodogram, i.e. 2.40673 hours (we excluded in this exercise the CRTS magnitudes associated to the recorded outburst; Section 2.2). The periodogram and corresponding CRTS folded light curve are shown on the top and middle panels of Figure 3, respectively. A double-humped modulation can be seen in the folded light curve which we identify as ellipsoidal modulation of the Roche-lobe filling donor. We then fitted an ephemeris to a set of 23 ( $\phi = 0 \pm 0.05$ ) timings, which resulted in

$$\text{HJD}(\phi = 0) = 2453383.578(1) + E \times 0.10028081(8), \quad (1)$$

where  $\phi = 0$  refers to the inferior conjunction of the donor star and HJD is the heliocentric Julian date (in days). We adopt the orbital period of SDSS J0011-0647 as the one obtained from the above photometric ephemeris, i.e. 2.40673946 hours.

We measured the radial velocities of the donor star by fitting a second order polynomial plus a double-Gaussian line profile of fixed separation to the  $\text{Na I } \lambda\lambda 8183.27, 8194.81 \text{ \AA}$  absorption doublet sampled by the MIKE spectra (see Rebassa-Mansergas et al. 2008 for

Table 1:  $\text{Na I } \lambda\lambda 8183.27, 8194.81 \text{ \AA}$  radial velocities of the donor star in SDSS J0011-0647. Heliocentric Julian dates, HJDs, are also provided. The radial velocities folded over the orbital period are shown in the bottom panel of Figure 3.

HJD	$\text{RV}_{\text{NaI}}$	err	HJD	$\text{RV}_{\text{H}\alpha}$	err
days	km/s		days	km/s	
2455737.8675	-58.6	26.6	2456192.5668	337.7	9.3
2455737.8749	122.4	18.4	2456192.5815	239.1	9.3
2455737.8828	251.7	36.9	2456192.5888	123.0	10.8
2455737.8902	331.6	17.7	2456192.6040	-173.4	7.7
2455737.8975	333.1	35.3	2456192.6257	-244.1	7.8
2455737.9065	302.7	34.0	2456192.6332	-171.9	7.7
2455737.9156	125.3	36.0	2456192.6405	-31.6	43.6
2455737.9264	-84.2	16.8	2456192.7190	-269.5	8.2
2456192.5521	207.3	27.7	2456193.6488	75.1	13.9
2456192.5593	327.0	88.2	2456193.6892	163.8	11.6



details). The donor star radial velocity values obtained in this way are provided in Table 1 and the radial velocity curve folded over the adopted value of the orbital period is shown in the bottom panel of Figure 3. We performed a sine-fit of the form

$$V_r = K_{\text{don}} \sin \left[ \frac{2\pi(t - T_0)}{P_{\text{orb}}} \right] + \gamma, \quad (2)$$

to the Na I  $\lambda\lambda 8183.27, 8194.81\text{\AA}$  absorption doublet folded radial velocity curve (dashed line in the bottom panel of Figure 3) to obtain the systemic velocity  $\gamma$  and the semi-amplitude velocity of the donor star  $K_{\text{don}}$  (where  $T_0$  and  $P_{\text{orb}}$  are the values provided by Equation 1). These values, together with our adopted value of the orbital period and  $T_0$ , are reported in Table 2.

### 3.2. Mass ratio and semi-amplitude velocity of the white dwarf

The high resolution spectra obtained with MIKE allowed us to measure the rotational broadening  $V_{\text{rot}}$  of the secondary star (affected by the inclination factor). The quantity  $V_{\text{rot}} \times \sin i$  is related to the mass ratio  $q$  via

$$V_{\text{rot}} \times \sin i = K_{\text{don}}(q + 1) \frac{R_{\text{don}}}{a} \quad (3)$$

(Horne et al. 1986), where for a Roche-lobe filling star  $R_{\text{don}}/a$  is a function of  $q$  (Eggleton 1983). We used this equation to calculate the mass ratio  $q$  and the white dwarf semi-amplitude velocity  $K_{\text{wd}}$ , which is simply given by  $K_{\text{wd}} = q \times K_{\text{don}}$ .

We measured the rotational broadening following the method described in Marsh et al. (1994). This method works via an optimal subtraction routine, in which a constant times a normalised and broadened template spectrum is subtracted from the normalised, orbitally

Table 2: Stellar and orbital parameters of SDSS J0011-0647. In order of appearance are the orbital period, the systemic velocity, the semi-amplitude velocity of the donor star, the semi-amplitude velocity of the white dwarf, the mass ratio, the time of inferior conjunction of the donor star, the mass of the white dwarf, the mass of the donor star and the orbital inclination.

---



---


$$P_{\text{orb}}[\text{h}] = 2.40673946 \pm 0.00000001$$

$$\gamma [\text{km/s}] = 28 \pm 3$$

$$K_{\text{don}} [\text{km/s}] = 310 \pm 4$$

$$K_{\text{wd}} [\text{km/s}] = 100 \pm 26$$

$$q = 0.32 \pm 0.08$$

$$T_0 [\text{HJD}] = 2453383.578 \pm 0.001$$

$$M_{\text{wd}} [M_{\odot}] > 0.65M_{\odot}$$

$$0.208M_{\odot} < M_{\text{don}} [M_{\odot}] < 0.447M_{\odot}$$

$$47 < i [^{\circ}] < 70$$


---

corrected target spectrum.  $V_{\text{rot}}$  is determined by finding the broadening factor which minimises the  $\chi^2$  between this residual spectrum and a smoothed version of itself.

Using our determinations of  $K_{\text{don}}$  and  $\gamma$  (Table 2), we applied an offset to each MIKE spectrum to remove the orbital variation and then averaged the spectra. We also obtained a series of six template stars of known spectral type and luminosity class which were observed as part of a different programme (HD217880 (G8 IV), HD215784 (K1 IV), HD163197 (K4 IV), HD220492 (G5 V), HD223121 (K1 V) and HD224287 (G8 V); D. Steeghs, private communication). We found the  $\text{Fe I } \lambda 5455.61 \text{ \AA}$  and  $\text{Fe I } \lambda 5615.64 \text{ \AA}$  absorption lines to be prominent in both the target and all the template spectra, and so use these lines for our  $V_{\text{rot}}$  determination. The template spectra cover a different wavelength range to the target, hence it was not possible to use more obvious spectral features like the  $\text{Na I } \lambda \lambda 8183.27, 8194.81 \text{ \AA}$  absorption doublet. These template spectra were re-binned to match the target spectrum, and we broadened the templates to account for smearing as a result of the orbital motion of the target. For each template star we then applied a range of rotational broadenings and computed  $\chi^2$  curves using the optimal subtraction method. Using the two Fe I absorption lines we obtained a consistent measurement of  $V_{\text{rot}}$  with all six templates, but for the G stars the templates did not match the target spectrum as well as the K stars and subsequently the fits were poorer, thus we excluded them from further consideration. Figure 4 shows the resulting  $\chi^2$  curves when considering the  $\text{Fe I } \lambda 5615.64 \text{ \AA}$  line for our K star templates. The minima of these curves give the preferred values of  $V_{\text{rot}} \times \sin i$  for the cases where the donor star in the CV is of the same type as the template star.

$q$  and  $K_{\text{wd}}$  obtained from each template using Equation 3 are given in Table 3. In this table we also provide the quantity  $\chi_{\text{min}}^2 - \chi_{\text{global}}^2$ , where  $\chi_{\text{min}}^2$  gives the preferred value of  $V_{\text{rot}} \times \sin i$  for each template and  $\chi_{\text{global}}^2$  is the global  $\chi_{\text{min}}^2$ . Inspection of Table 3 and Figure 4 reveals that the inferred  $q$  and  $K_{\text{wd}}$  values from the three templates are in good

agreement, however the best fit is obtained when we use HD 215784 (see also Figure 5), which has a spectral type of K1 IV, as the template star. We therefore adopt  $q$  and  $K_{\text{wd}}$  as those obtained using this star. The adopted  $q$  and  $K_{\text{wd}}$  values are also reported in Table 2.

Based on the multiplicative factor used when we fit the template to the observed spectra we can also estimate the relative contribution of the donor star, which is found to be  $37 \pm 10$  per cent when we use HD 215784 (spectral type K1 IV, our best-fitting template star). Since the contribution from the white dwarf at this wavelength is expected to be small ( $\sim 3 - 5$  per cent, see Section 3.4 for a further discussion on this issue), the disk contribution should be  $\sim 60 - 70$  per cent. The relative contribution of the donor star is found to be  $30 \pm 9$  per cent and  $45 \pm 13$  per cent when we use our two other template stars HD 163197 (K4 IV) and HD 223121 (K1 V), respectively, i.e. disk contributions of  $\sim 65 - 75$  per cent and  $\sim 50 - 60$  per cent.

### 3.3. Orbital inclination and stellar masses

With knowledge of the orbital period, radial velocity semi-amplitudes and mass ratio (Table 2) we can place a lower limit on the binary inclination using Kepler’s laws and the fact that the white dwarf should have a mass less than the Chandrasekhar mass,

$$M_{\text{wd}} = \frac{K_{\text{don}} P_{\text{orb}} (1 + q)^2}{2\pi G \sin i^3} < 1.4 M_{\odot}. \quad (4)$$

Using our measured values of  $K_{\text{don}}$ ,  $P_{\text{orb}}$  and  $q$  gives a limit on the inclination of  $i > 47^\circ$ . This limit, and the mass ratio, also tells us that the mass of the donor star is  $M_{\text{don}} < 0.447 M_{\odot}$ .

We can place further constraints on the system parameters using our Ultracam  $g'$  and  $r'$  band light curves (the  $u'$  band light curve is of low quality and therefore not considered in this exercise). These light curves, folded over the ephemeris provided in Equation 1, are shown in Figure 6. Unfortunately, we did not cover a whole orbital cycle and hence there is

a small gap in phase coverage. Inspection of Figure 6 reveals the light curves display a clear sinusoidal variation with a period of half that of the binary itself. This variation is also present in the CRTS light curve (Figure 3, middle panel) and is caused by the ellipsoidally distorted donor star presenting different surface areas towards us throughout its orbit. Furthermore, it is clear that the minima at phase 0.5 are much lower than at phase 1.

We fitted the Ultracam light curves using a code developed specifically for modeling binaries containing white dwarfs (Copperwheat et al. 2010). The code accounts for Roche distortion and we included both a disk and bright spot component in our model. The disk contribution is essentially constant throughout the orbit, whilst the bright spot contribution rises around phase 1 when it is directed towards the observer and disappears around phase 0.5 when its light is moving away from us. Therefore, it can naturally account for the differences in the depths of the two minima in the light curve, by decreasing the depth of the phase 1 minimum. The white dwarf in SDSS J0011-0647 contributes a small amount of flux in the  $g'$  and  $r'$  bands (see Section 3.4 for a further discussion on this issue).

We set the mass ratio to our spectroscopically measured value (Table 2) and fixed the donor star’s radius to its Roche lobe. We allowed the disk contribution to vary and the bright spot’s contribution and orientation to vary as well. We fitted the light curves using Levenberg-Marquardt minimisation. We increased the inclination in steps of  $1^\circ$  from  $47^\circ$  (the minimum inclination based on the white dwarf’s mass) up to  $90^\circ$ . We emphasise that our aim is not to determine the exact inclination, but rather to set an upper limit on the inclination, above which the disk and bright spot are eclipsed (which is ruled out by the light curves).

The best fits to the light curves are shown in Figure 6. We also show the individual components (donor star, disk and bright spot). We find that at inclinations larger than  $70^\circ$  the eclipse of the disk and bright spot is large enough so that we should have detected it

in our light curves, hence we can place this upper limit on the inclination. Generally, at inclinations where there is no eclipse, the light curve is fairly insensitive to the inclination, since the contributions from the donor and disk can be varied to account for any differences. This effect can be seen in Figure 6, where the contributions from the individual components resulting from our best fits to the two light curves are different. Moreover, we find that even for very high inclinations (i.e. eclipsing) the disk contributions from our best fits ( $\sim 10 - 20$  per cent, depending on the considered light curve, see Figure 6) are lower than the spectroscopically estimated value ( $\sim 60 - 70$  per cent, section 3.2). This fact, along with the possibility of star-spots on the donor (which could also account for the varying depths of the light curve minima, and were not included in our model) means that we are unable to put any tighter constraints on the inclination.

Figure 7 shows the masses of both the white dwarf and donor star as a function of inclination, as well as our limits on the inclination. We find that the mass of the white dwarf is  $M_{\text{wd}} > 0.65M_{\odot}$ , and the mass of the donor star is  $0.208M_{\odot} < M_{\text{don}} < 0.447M_{\odot}$ . We include these values also in Table 2.

### 3.4. Spectral type of the secondary star

The mass of the donor star of SDSS J0011-0647 is  $0.21-0.45M_{\odot}$  (Section 3.3), which corresponds to a spectral type of M5.5–1.5 if we assume a zero-age main sequence star (Rebassa-Mansergas et al. 2007, see their Table 5). However, our analysis indicates a substantially hotter spectral type for this star (Section 3.2). To investigate this hypothesis further we considered a set of nine G,K,M donor star template spectra<sup>1</sup>, combined them

---

<sup>1</sup>Our main sequence template spectra include six SEGUE (the SDSS Extension for Galactic Understanding and Exploration, Yanny et al. 2009) G and K stars of spectral types de-

with white dwarf model spectra (Koester 2010) and the emission from an isobaric and isothermal hydrogen slab as an approximation of the emission from the accretion disk (Gänsicke et al. 1999), and compared the resulting combined (donor star plus accretion disk plus white dwarf) spectra to the SDSS optical spectrum and Galaxy Evolution Explorer (*GALEX*, Martin et al. 2005; Morrissey et al. 2005) ultraviolet fluxes of SDSS J0011-0647.

For a given donor star template, the resulting combined spectrum depended on the white dwarf effective temperature and surface gravity (or mass) assumed, on the choice of the accretion disk’s gas pressure and temperature and its optical depth (where the latter relied on the height of the isothermal hydrogen slab and the inclination of the disk considered), and on the corresponding contributions to the total flux of the three individual components (white dwarf, accretion disk and donor star). It is important to keep in mind that our aim here is not to determine all these physical characteristics of SDSS J0011-0647, as the large number of free parameters would result in significant degeneracies, but rather to investigate whether or not combinations of these parameters exist that match well the observed spectrum, and use these results to constrain the spectral type of the donor star. Thus, in order to reduce the large number of free parameters involved, we fixed the white dwarf mass to  $0.7M_{\odot}$  and the inclination of the accretion disk to  $67^{\circ}$  (values that result from the best-model fit to our Ultracam light curves, Section 3.3) and considered  $10^8$  cm as the hydrogen slab’s height in all fits, thus fixing also the optical depth of the accretion disk. To facilitate the comparison the observed and combined spectra (as well as the *GALEX* ultraviolet fluxes) were normalised to  $5615.64\text{\AA}$ , where the contribution of the accretion disk is estimated to be  $\sim 60 - 70$  per cent (Section 3.2). For each donor star template we visually explored a large number of composite models, spanning a representative range in

---

terminated by the MILES library (Sánchez-Blázquez et al. 2006) and three M stars from the library of Rebassa-Mansergas et al. (2007).

all free parameters, and computed a reduced  $\chi^2$  for each model. In each individual fit the *GALEX* ultraviolet fluxes of SDSS J0011-0647 were used to directly constrain the white dwarf effective temperature and its contribution to the total combined flux. We report in Table 4 the parameters resulting in the lowest  $\chi^2$  for each of the donor star templates, and show the corresponding composite models along with the observations of SDSS J0011-0647 in Figure 8.

Inspection of Figure 8 and Table 4 reveals that the best combined fits to the observed spectrum of SDSS J0011-0647 are obtained when we use the K4 V and G8 IV template stars, even though reasonably good fits are also obtained for the K1 IV and K1 V templates. This corroborates, overall, our previous findings, i.e. that the donor star has a spectral type that is much earlier than expected for its mass. The quality of the fits deteriorates when adopting the later spectral types K7 V and M0 V, and the worst fits are obtained for the M3 V, M5 V and G8 V templates. It is worth noting that the accretion disk contributions are found to be  $\sim 40 - 55$  per cent for the best-matching donor star templates (falling between the previous spectroscopic estimated value of  $\sim 60 - 70$  per cent, Section 3.2, and the photometric obtained value of  $\sim 10 - 20$  per cent, Section 3.3), however the disk contributions increase considerably for the worse-fitting donor star templates K7 V, G8 V, M0 V, M3 V and M5 V (Table 4). This effect is simple to understand: when adopting a donor star template that does not match the observed spectrum of SDSS J0011-0647, our fit decreases the contribution of the donor star to the composite model, the contribution of the disk is increased to compensate, and the disk temperature is optimized such that the quasi-blackbody spectrum of the disk approximates the observed data. The most noticeable feature that the early-to-mid K star templates reproduce well is the strong Mg I absorption complex near  $5150\text{\AA}$ . This feature is weak, or absent, in the earlier and later donor stars, as well as in any accretion disk model. We investigate the diagnostic strength of the Mg I absorption in more detail by comparing the  $\chi^2$  values obtained in the  $3850\text{-}6000\text{\AA}$



wavelength range (designated as  $\chi_b^2$  in Table 4), where the observed spectrum displays both spectral features and continuum. Clearly, the best-combined fits which provide the lowest  $\chi^2$ -fit values (those in which the donor star template is a K4 V, G8 IV, K1 IV and K1 V) provide also the lowest  $\chi_b^2$ -fit values.

We conclude that spectral types later than K7 V and earlier than G8 V can be ruled out for the donor star of SDSS J0011-0647. This confirms in a robust way our previous finding, i.e. that this star is clearly too hot for its mass. In the following section we discuss in detail the implications of this peculiarity on the evolution of SDSS J0011-0647. We also find that, as expected, the white dwarf contribution to the optical flux of SDSS J0011-0647 is small (3-5 per cent at 5615.64Å, Table 4), and that its effective temperature is  $\sim$ 14000-16000 K.

#### 4. Discussion and conclusions

SDSS J0011-0647 is peculiar CV in which the donor star is substantially hotter (the observations are best-matched with an early-to-mid K star) than expected for its mass (0.21–0.45 $M_\odot$ ), one of the most extreme cases among CVs of its kind. The present-day configuration of these peculiar CVs can be explained if the donor stars underwent substantial nuclear evolution before reaching contact (Beuermann et al. 1998; Baraffe & Kolb 2000; Schenker et al. 2002; Podsiadlowski et al. 2003). This is only possible if at the onset of mass transfer the secondary star of SDSS J0011-0647 was considerably more massive than the mass of canonical CV donors. Hence, it is almost certain that SDSS J0011-0647 passed through a substantial phase of thermal-timescale mass transfer, during which it might have been expected to appear as a super-soft source (Schenker et al. 2002). Super-soft X-ray sources are a viable channel to produce type Ia supernovae (SN Ia, van den Heuvel et al. 1992; Rappaport et al. 1994; Li & van Den Heuvel 1997; Starrfield et al. 2004; Di Stefano 2010). Although SDSS J0011-0647 obviously failed at producing a SN Ia during this intense

phase of thermal transfer mass transfer, its prior evolution may help to test models of SN Ia progenitors, i.e. if we were able to somehow estimate the original mass of the white dwarf, then the present-day component masses would constrain the accretion efficiency of the white dwarf during that super-soft phase (Rodríguez-Gil et al. 2009). However, the arguments are only likely to be indirect.

Depending on the degree of hydrogen depletion in the center, evolved donor stars are not expected to become fully convective (Baraffe & Kolb 2000). Therefore they should not be subject to the same disruption of magnetic braking as the donor stars in canonical CVs. These peculiar CVs are thus not expected to detach in the orbital period gap between 2-3 hours. The orbital period of SDSS J0011-0647 is in the middle of the period gap, thereby providing direct observational evidence supporting the models for these hot donor stars. Arguably, this also provides indirect support for the belief that the period gap arises as a consequence of the secondary stars in normal CVs becoming fully convective. Future tests of the angular momentum loss in SDSS J0011-0647 may be able to test magnetic braking in a previously unexplored regime.

These CVs with evolved donor stars are also predicted to later become AM CVn-like binaries (Schenker et al. 2002; Podsiadlowski et al. 2003). Further, more detailed, measurements of the properties of SDSS J0011-0647 would thus help to refine current models describing this evolutionary phase. For example, future photometric near-infrared observations are likely to constrain considerably the orbital inclination (and therefore the stellar masses, Figure 7) of SDSS J0011-0647, as the disk contribution to the ellipsoidal modulation is essentially negligible at these wavelengths. In addition, it is possible to indirectly measure the mass of the white dwarf from ultraviolet (e.g. HST) spectroscopic observations.

Furthermore, SDSS J0011-0647 may help in constraining population models that

describe the evolution of these peculiar CVs (Baraffe & Kolb 2000; Schenker et al. 2002; Podsiadlowski et al. 2003). It is worth noting that these models have not predicted many, if any, systems with similar donor temperatures (or spectral types) to SDSS J0011-0647 at the same orbital period. This may indicate that the specific properties of SDSS J0011-0647 require unexpected or rare initial conditions. For example, the binary grids used by Podsiadlowski et al. (2003) may not have been able to predict the existence of systems resembling SDSS J0011-0647 either because the upper limit to the donor mass ( $1.4M_{\odot}$ ) was too low or because the spacing in initial period was insufficiently tight, i.e. either the initial parameter space was not large enough or not sufficiently finely-sampled. In particular, since the necessary orbital period at contact may have been close to the bifurcation period beyond which systems would become wider rather than tighter (see, e.g. Pylyser & Savonije 1988), some careful fine-tuning may be required when setting up grids of binary evolution sequences in order to cover the part of parameter space which produced SDSS J0011-0647.

Combining SDSSJ170213.26+323954.1 (Littlefair et al. 2006a), CSS J134052.0+151341 (Thorstensen 2013) and the system we have discovered makes three peculiar CVs containing hot donor stars which have near-identical orbital periods ( $\approx 2.4$  hours). To this sample we could add the recurrent nova IM Nor (2.462 h; Woudt & Warner 2003), as formation models for the recurrent novae with short orbital periods typically involve a similar phase of thermal-timescale mass transfer onto the white dwarf (see, e.g., Podsiadlowski 2003; Sarna et al. 2006) (although the spectral type of the donor of IM Nor is unknown). Only one other peculiar CV containing a hot donor, QZ Serpentis (Thorstensen et al. 2002a), is known in the period gap (and that is at the very short-period edge of the gap). This implies  $\sim 1/2$  of the total currently-observed sample of these peculiar CVs are located in the period gap, and  $4/5$  of those (if we include also IM Nor) with nearly the same orbital period. Even though we are subject to low number statistics, this concentration of systems at a particular orbital period within the period gap may deserve further attention.

*Acknowledgments: This work is dedicated to our friend Dr. Gisela Andrea Romero, may she rest in peace. We thank Andrew Drake for providing us the Catalina Real-Time Transient Survey images of SDSS J001153.08-064739.2, Danny Steeghs for providing us G and K star template spectra observed with Magellan Clay/MIKE, and the anonymous referee for his/her comments and suggestions. ARM acknowledges financial support from the Postdoctoral Science Foundation of China (grant 2013M530470) and from the Research Fund for International Young Scientists by the National Natural Science Foundation of China (grant 11350110496). SGP acknowledges financial support from FONDECYT in the form of grant number 3140585. SJ thanks Philipp Podsiadlowski for discussions and CAS and NSFC (Grant No. 11350110324) for support. MRS thanks for support from FONDECYT (grant 1141269). TRM acknowledges financial support from STFC grant ST/L000733/1. The research leading to these results has received funding from the European Research Council under the European Union’s Seventh Framework Programme (FP/2007-2013) / ERC Grant Agreement n. 320964 (WDTracer).*

Table 3: Template spectra used for measuring the rotational broadening of the donor star in SDSSJ0011-0647. The second column indicates the spectral type of each template. The third, fourth and fifth columns give the measured rotational broadening and the inferred  $q$  and  $K_{\text{wd}}$ , respectively. In the last column we provide the quantity  $\chi_{\text{min}}^2 - \chi_{\text{global}}^2$ , where  $\chi_{\text{min}}^2$  is the minimum of the  $\chi^2$  curve obtained from each template (Figure 4) and  $\chi_{\text{global}}^2$  is the global minimum among all  $\chi_{\text{min}}^2$ . HD 215784 provides the best fit ( $\chi_{\text{min}}^2 - \chi_{\text{global}}^2=0$ , see also Figure 5).

Template	Sp	$V_{\text{rot}} \times \sin i$ km/s	$q$	$K_{\text{wd}}$ km/s	$\chi_{\text{min}}^2 - \chi_{\text{global}}^2$
HD 215784	K1 IV	$117 \pm 15$	$0.32 \pm 0.08$	$100 \pm 26$	0
HD 163197	K4 IV	$118 \pm 12$	$0.33 \pm 0.07$	$101 \pm 20$	3.9
HD 223121	K1 V	$106 \pm 17$	$0.26 \pm 0.09$	$82 \pm 28$	6.2

Table 4: Set of parameters that allow the best combined fit (donor star template plus accretion disk model spectrum plus white dwarf model spectrum; see Figure 8) to the optical spectrum and *GALEX* ultraviolet fluxes of SDSS J0011-0647. In all cases the white dwarf mass is fixed to  $0.7M_{\odot}$ , and the inclination of the disk to  $67^{\circ}$ . The contribution of each component to the total combined flux model at  $5615.64\text{\AA}$  is also indicated. The last two columns indicate the  $\chi^2$  values that result from comparing the best-fit combined model and the observed spectrum for the entire optical wavelength range ( $\chi_{\text{all}}^2$ ) and for the blue range of the optical spectrum ( $\chi_{\text{b}}^2$ , 3850-6000 $\text{\AA}$ ), respectively.

Template donor	$T_{\text{WD}}$	$P_{\text{disk}}$	$T_{\text{disk}}$	WD	Donor	Disk	$\chi_{\text{all}}^2$	$\chi_{\text{b}}^2$
	[K]	[dyn/cm <sup>2</sup> ]	[K]	Contr.	Contr.	Contr.		
				[%]	[%]	[%]		
K4 V	14000	300	5000	5	55	40	26	39
G8 IV	16000	500	5200	3	44	53	37	60
K1 IV	16000	800	5200	3	43	54	54	65
K1 V	16000	200	4600	3	51	46	46	79
G8 V	17000	200	4600	3	28	69	89	109
K7 V	14000	800	4800	5	13	82	65	112
M0 V	15000	800	4800	4	12	84	61	106
M5 V	15000	800	4800	4	1	95	89	159
M3 V	15000	800	4800	4	3	93	96	172

## REFERENCES

- Abazajian et al. 2009, *ApJS*, 182, 543
- Aihara et al. 2011, *ApJS*, 195, 26
- Augusteijn, T., Van Der Hooft, F., De Jong, J. A., & Van Paradijs, J. 1996, *A&A*, 311, 889
- Baraffe, I. & Kolb, U. 2000, *MNRAS*, 318, 354
- Beuermann, K., Baraffe, I., Kolb, U., & Weichhold, M. 1998, *A&A*, 339, 518
- Copperwheat, C. M., Marsh, T. R., Dhillon, V. S., Littlefair, S. P., Hickman, R., Gänsicke, B. T., & Southworth, J. 2010, *MNRAS*, 402, 1824
- Dhillon et al. 2007, *MNRAS*, 378, 825
- Di Stefano, R. 2010, *ApJ*, 712, 728
- Drake et al. 2009, *ApJ*, 696, 870
- Eggleton, P. P. 1983, *ApJ*, 268, 368
- Gänsicke, B. T. 2004, in *Compact Binaries and Beyond*, ed. G. Tovmassian & E. Sion, Conf. Ser. No. 20 (RMAA), 152–154
- Gänsicke et al. 2009, *MNRAS*, 397, 2170
- Gänsicke, B. T., Sion, E. M., Beuermann, K., Fabian, D., Cheng, F. H., & Krautter, J. 1999, *A&A*, 347, 178
- Gänsicke et al. 2003, *ApJ*, 594, 443
- Horne, K., Wade, R. A., & Szkody, P. 1986, *MNRAS*, 219, 791
- Imada et al. 2006, *PASJ*, 58, 143

- Kato, T. & Osaki, Y. 2014, ArXiv e-prints
- Knigge, C., Baraffe, I., & Patterson, J. 2011, ApJS, 194, 28
- Koester, D. 2010, Mem. Soc. Astron. Italiana, 81, 921
- Li, X. D. & van Den Heuvel, E. P. J. 1997, A&A, 322, L9
- Littlefair, S. P., Dhillon, V. S., Marsh, T. R., & Gänsicke, B. T. 2006a, MNRAS, 371, 1435
- Littlefair, S. P., Dhillon, V. S., Marsh, T. R., Gänsicke, B. T., Southworth, J., & Watson, C. A. 2006b, Science, 314, 1578
- Marsh, T. R., Robinson, E. L., & Wood, J. H. 1994, MNRAS, 266, 137
- Martin et al. 2005, ApJ, 619, L1
- Morrissey et al. 2005, ApJ, 619, L7
- Paczyński, B. 1981, Acta Astronomica, 31, 1
- Parsons et al. 2013, MNRAS, 429, 256
- Podsiadlowski, P. 2003, ArXiv Astrophysics e-prints
- Podsiadlowski, P., Han, Z., & Rappaport, S. 2003, MNRAS, 340, 1214
- Pylyser, E. & Savonije, G. J. 1988, A&A, 191, 57
- Rappaport, S., Di Stefano, R., & Smith, J. D. 1994, ApJ, 426, 692
- Rappaport, S., Joss, P. C., & Verbunt, F. 1983, ApJ, 275, 713
- Rappaport, S., Joss, P. C., & Webbink, R. F. 1982, ApJ, 254, 616
- Rebassa-Mansergas, A., Agurto-Gangas, C., Schreiber, M. R., Gänsicke, B. T., & Koester, D. 2013a, MNRAS, 433, 3398



- Rebassa-Mansergas, A., Gänsicke, B. T., Rodríguez-Gil, P., Schreiber, M. R., & Koester, D. 2007, MNRAS, 382, 1377
- Rebassa-Mansergas, A., Gänsicke, B. T., Schreiber, M. R., Koester, D., & Rodríguez-Gil, P. 2010, MNRAS, 402, 620
- Rebassa-Mansergas et al. 2008, MNRAS, 390, 1635
- Rebassa-Mansergas, A., Nebot Gómez-Morán, A., Schreiber, M. R., Gänsicke, B. T., Schwobe, A., Gallardo, J., & Koester, D. 2012, MNRAS, 419, 806
- Rebassa-Mansergas, A., Schreiber, M. R., & Gänsicke, B. T. 2013b, MNRAS, 429, 3570
- Rodríguez-Gil et al. 2009, A&A, 496, 805
- Sánchez-Blázquez 2006, MNRAS, 371, 703
- Sarna, M. J., Ergma, E., & Gerskevits, J. 2006, Acta Astron., 56, 65
- Schenker, K., King, A. R., Kolb, U., Wynn, G. A., & Zhang, Z. 2002, MNRAS, 337, 1105
- Schreiber et al. 2010, A&A, 513, L7+
- Schwarzenberg-Czerny, A. 1996, ApJ, 460, L107
- Starrfield, S., Timmes, F. X., Hix, W. R., Sion, E. M., Sparks, W. M., & Dwyer, S. J. 2004, ApJS, 612, L53
- Thorstensen, J. R. 2013, PASP, 125, 506
- Thorstensen, J. R., Fenton, W. H., Patterson, J., Kemp, J., Halpern, J., & Baraffe, I. 2002a, PASP, 114, 1117
- Thorstensen, J. R., Fenton, W. H., Patterson, J. O., Kemp, J., Krajci, T., & Baraffe, I. 2002b, ApJ, 567, L49

van den Heuvel, E. P. J., Bhattacharya, D., Nomoto, K., & Rappaport, S. A. 1992, *A&A*, 262, 97

Verbunt, F. & Zwaan, C. 1981, *A&A*, 100, L7

Woudt, P. A. & Warner, B. 2003, *MNRAS*, 343, 313

Yanny et al. 2009, *AJ*, 137, 4377

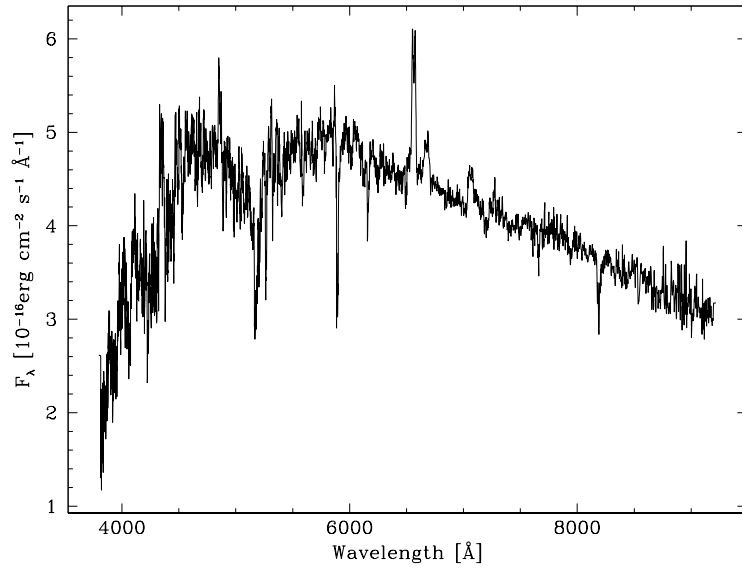


Fig. 1.— SDSS spectrum of SDSS J0011-0647 revealing the spectral features of the donor star and double-peaked Balmer emission lines characteristic of an accretion disk. No obvious white dwarf features can be seen.

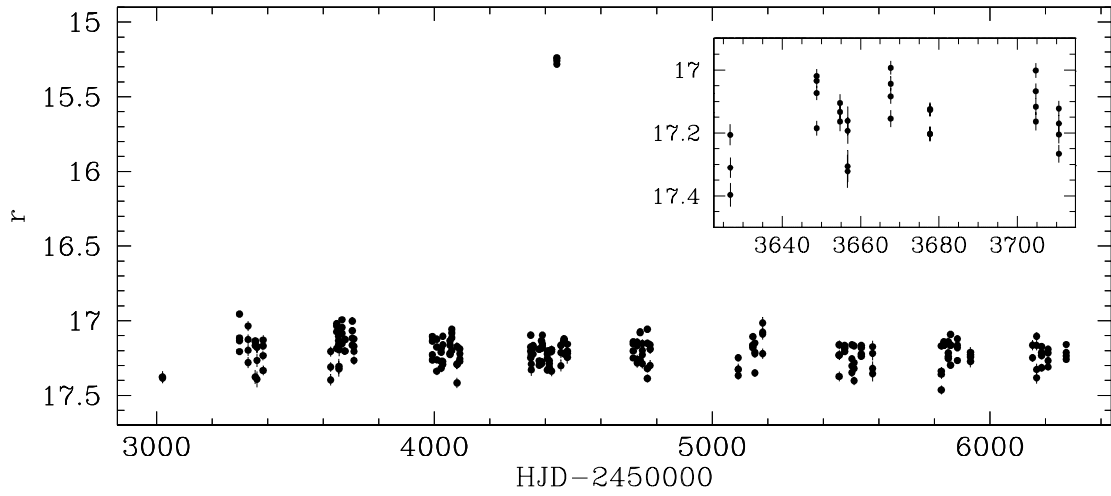


Fig. 2.— CRTS light curve of SDSS J0011-0647. The decrease from  $r \sim 17$  to  $r \sim 15$  is due to SDSS J0011-0647 undergoing an outburst. A zoom-in of 84 days is provided in the top right corner of the figure. The data folded over the orbital period of the binary can be seen in Figure 3.

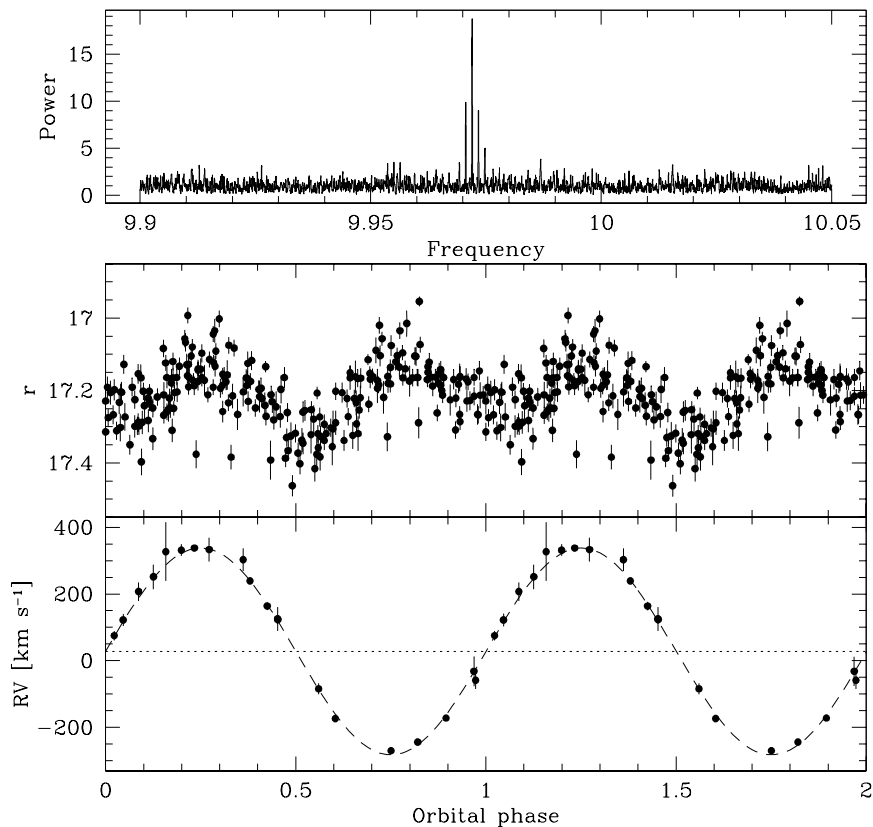


Fig. 3.— Top: power spectra obtained applying an ORT periodogram to the CRTS photometry of SDSS J0011-0647, indicating an orbital period of 2.40673 hours. Middle: the CRTS light curve folded over the orbital period. Bottom: Na I  $\lambda\lambda$  8183.27,8194.81Å (black solid dots, originated on the donor star) radial velocities folded over our adopted value of the orbital period and best sine-fit to the data (dashed line). The horizontal dotted line represents the systemic velocity.

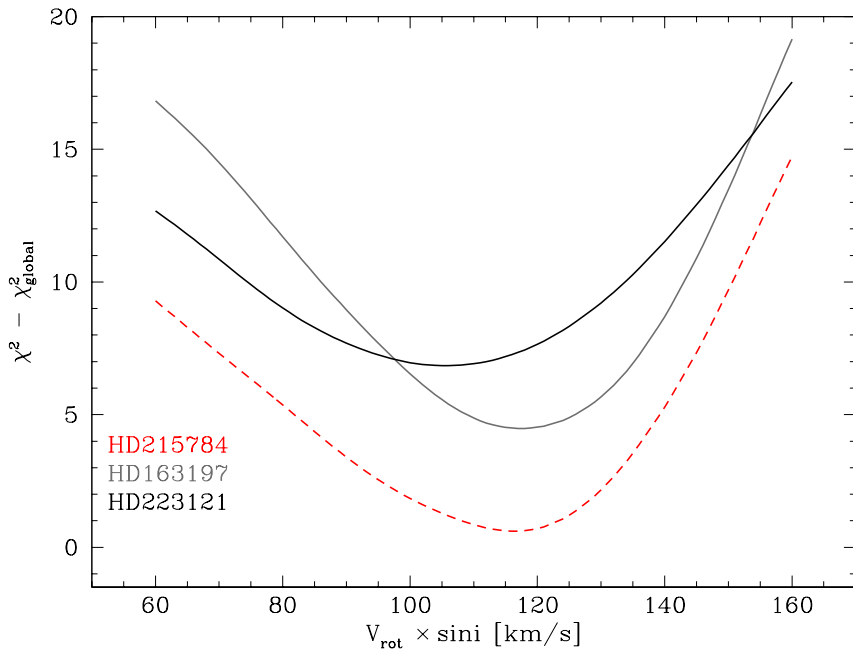


Fig. 4.— Rotational broadening measured fitting the template spectra to the averaged observed spectrum of SDSS J0011-0647 as a function of  $\chi^2 - \chi_{\text{global}}^2$ , where  $\chi_{\text{global}}^2$  is the global  $\chi^2$  minimum ( $\chi_{\text{min}}^2$ ) among all curves. The best value of the rotational broadening corresponds in each case to  $\chi_{\text{min}}^2$  (see Table 3). Uncertainties are assumed as the maximum difference between the values below  $\chi^2 - \chi_{\text{min}}^2 = 1$ . The best fit is obtained when we use HD215784 as the template star (red dashed line).

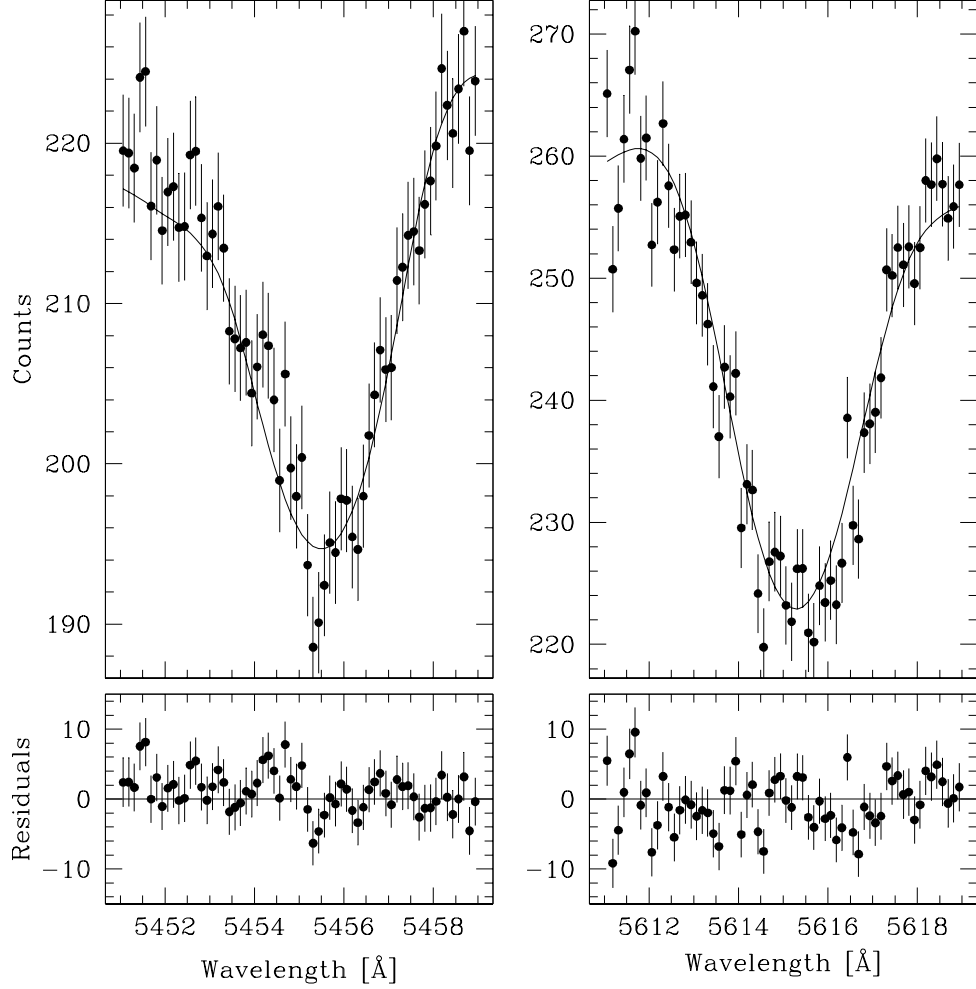


Fig. 5.— Two Fe I absorption lines in the orbitally shifted and averaged spectrum of SDSS J0011-0647. The solid line plotted over the data points is the spectrum of our best fitting template star (HD 215784), which has been artificially broadened by a factor  $V_{\text{rot}} \times \sin i = 117$  km/s and fitted to our data via an optimal subtraction routine as described in Section 3.2.

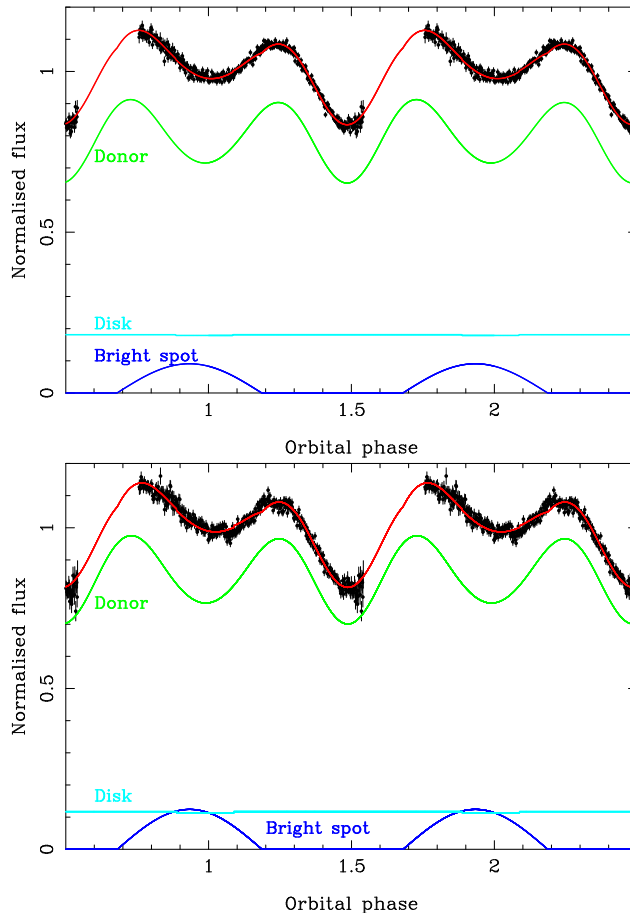


Fig. 6.— ULTRACAM  $r'$  band (top) and  $g'$  band (bottom) light curves of SDSS J0011-0647. Over-plotted are the best fit models (red). We also show the relative contributions of the donor star (green), disk (cyan) and bright spot (blue) in these models. These contributions vary depending on the considered band. Our best models have an inclination of  $67^\circ$  and the disk is just eclipsed (note the small dip in the disk light curves around phase 1). At inclinations above  $70^\circ$  this eclipse would be deep enough to be detectable in our data.



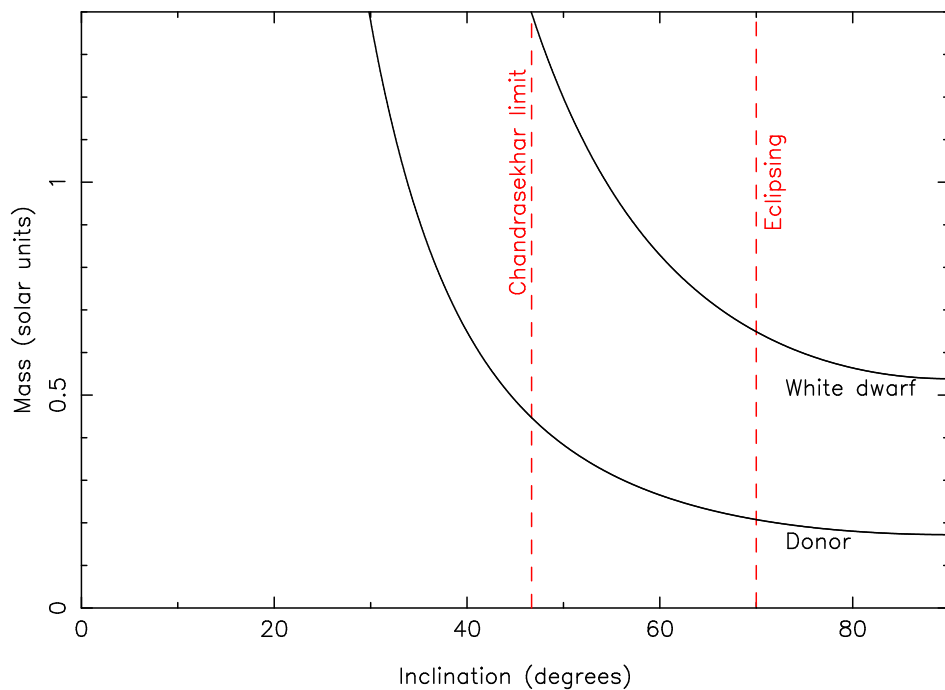


Fig. 7.— Mass function plot for both the white dwarf and donor star in SDSS J0011-0647. A lower limit on the inclination of  $47^\circ$  is placed by insisting that the white dwarf mass be lower than the Chandrasekhar limit. The lack of any disk or bright spot eclipse in the light curve places an upper limit on the inclination of  $70^\circ$ .

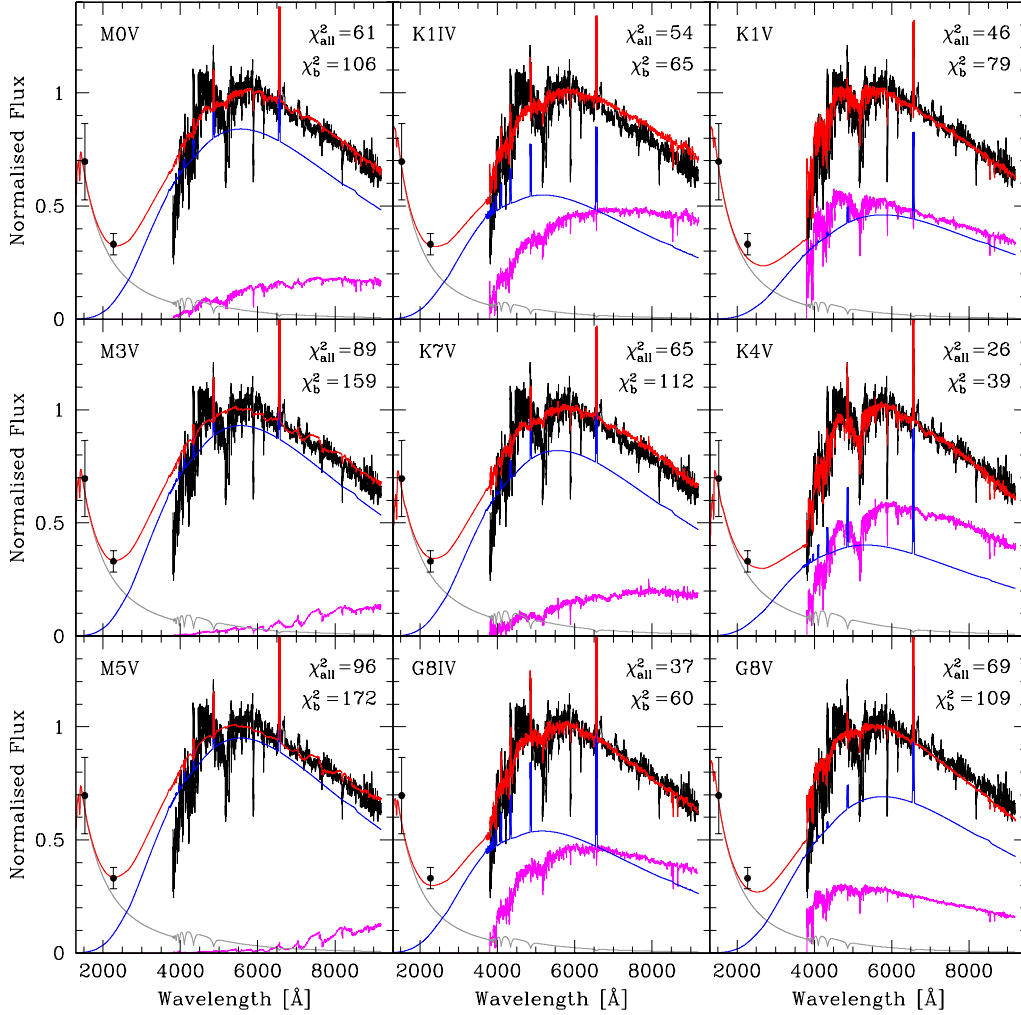


Fig. 8.— Comparison of the normalised SDSS optical spectrum (black) plus *GALEX* ultraviolet fluxes (black solid dots) of SDSS J0011-0647 to a set of combined donor star template (magenta), white dwarf model spectra (gray) and accretion disk model spectra (blue; red for the total combined model, also normalised). The spectral types of the donor star templates used and the  $\chi^2$  that result from comparing the combined model to the observed spectra are also indicated (where  $\chi^2_{\text{all}}$  is the  $\chi^2$  obtained using the entire optical range and  $\chi^2_{\text{b}}$  is the  $\chi^2$  obtained considering only the 3850-6000Å range). A spectral type later than K7V can be ruled out for the donor star, which confirms in a robust way this star is too hot for its inferred mass (Figure 7).